Comparison of PARASOL observations with polarized reflectances simulated using different ice habit mixtures

Benjamin H. Cole[1*], Ping Yang[1], Bryan A. Baum[2],

Jerome Riedi[3], Laurent C.-Labonnote[3], Francois Thieuleux[3] , Steven Platnick[4]

1. Department of Atmospheric Sciences, Texas A&M University, College Station, TX , USA

2. Space Science and Engineering Center, University of Wisconsin-Madison, Madison, WI, USA

3. Laboratoire d'Optique Atmosphérique, Universite des Sciences et Technologies de Lille/CNRS, Villeneuve d'Ascq, France.

4. NASA Goddard Space Flight Center, Greenbelt, MD, USA

For publication in the

Journal of Applied Meteorology and Climatology

Corresponding author address: Benjamin H. Cole, Department of Atmospheric Sciences, Texas A&M University, 3150 TAMU, College Station, TX 77843, USA. Email: ben.cole@tamu.edu

Abstract

Insufficient knowledge of the habit distribution and the degree of surface roughness of ice crystals within ice clouds is a source of uncertainty in the forward light scattering and radiative transfer simulations required in downstream applications involving these clouds. The widely used MODderate resolution Imaging Spectroradiometer (MODIS) Collection 5 ice microphysical model assumes a mixture of various ice crystal shapes with smooth-facets except aggregates of columns for which a moderately rough condition is assumed. When compared with PARASOL (Polarization and Anisotropy of Reflectances for Atmospheric Sciences coupled with Observations from a Lidar) polarized reflection data, simulations of polarized reflectance using smooth particles show a poor fit to the measurements, whereas very rough-faceted particles provide an improved fit to the polarized reflectance. In this study a new microphysical model based on a mixture of 9 different ice crystal habits with severely roughened facets is developed. Simulated polarized reflectance using the new ice habit distribution is calculated using a vector adding-doubling radiative transfer model, and the simulations closely agree with the polarized reflectance observed by PARASOL. The new general habit mixture is also tested using a spherical albedo differences analysis, and surface roughening is found to improve the consistency of multi-angular observations. It is suggested that an ice model incorporating an ensemble of different habits with severely roughened surfaces would potentially be an adequate choice for global ice cloud retrievals.

Introduction

Ice clouds play an important role in regulating the energy balance of the Earth (Liou 1986), with a frequency of occurrence approaching 70% in tropical regions (Nazaryan et al. 2008). The ice cloud microphysics largely determines the radiative properties of these clouds, but current knowledge of ice cloud microphysics is still limited (Baran 2009). Cloud modeling and comparison with remote sensing observations can be used to investigate the properties of ice clouds and reduce uncertainties in their microphysical properties. In current operational ice cloud retrievals using the MODderate resolution Imaging Spectroradiometer (MODIS) satellite, the collection 5 ice cloud model (Baum et al. 2005b) is used. This model consists of six different particle shapes (habits) and smooth surfaces for all the habits, except for the aggregates consisting of severely roughened solid columns. To improve the MODIS collection 5 model, a new ice model incorporating 9 different ice habits with severely roughened facets is suggested in this study. In addition to the ice crystal habits in the MODIS collection 5 model, the new model incorporates three new ice habits: a hollow bullet rosette and a small and large aggregate of plates.

Chepfer et al. (1998) showed that polarization is sensitive to the shape of ice crystals, so to examine the impact of the new ice model, simulations of polarized reflectance from an optically thick ice cloud ($\tau = 5$) are compared with PARASOL multi-angle polarized reflectance measurements. The adding-doubling model of de Haan et al. (1987) is employed to simulate the polarized reflectance at the top of the atmosphere (TOA). The single-scattering properties of the ice crystals were taken from a new database that provides the spectrally consistent optical properties of ice particles from ultraviolet to far-infrared wavelength regimes (Yang et al. 2012), and the bulk scattering properties are calculated

following Baum et al. (2005b). In addition, a Spherical Albedo Differences (SAD) analysis (C.-Labonnote et al. 2001) is performed to investigate the angular consistency of the ice cloud model. The SAD analysis consists of inferring cloud optical thickness τ at various observation angles and subsequently testing the consistency of the cloud spherical albedo derived from these τ values.

The remainder of this paper contains the following sections: section 2 outlines the data used and the radiative transfer (RT) model employed to do the simulations for the polarized reflectance analysis; section 3 presents the results of the comparison of model simulations of polarized reflectance and spherical albedo difference to PARASOL satellite measurements; and section 4 summarizes the work.

2. Data and Models

2.1 The PARASOL satellite

The Polarization and Anisotropy of Reflectances for Atmospheric Sciences coupled with Observations from a Lidar (PARASOL) satellite is a French microsatellite launched in 2004 to study clouds and aerosols with multiple angle and polarization capabilities (Fougnie et al. 2007). It carries a derivative of the POLarization and Directionality of the Earth's Reflectances (POLDER) instrument, a wide-field imaging radiometer and polarimeter. This instrument has 9 bands, 3 of which have polarization capabilities. PARASOL views a given scene at up to 16 different angles as the satellite passes overhead. The polarization is achieved with filters at increments of 60° in a rotating wheel assembly (Deschamps et al. 1994). The measurements provide the I, Q, and U Stokes vector components, from which both cloud and aerosol properties may be inferred.

In this study, the Level-2 cloud product is used, which is based on the Level-1B radiances averaged over a larger spatial area (~18x18 km). Included in this product is the percentage cloud cover, surface type, cloud thermodynamic phase (ice, water, or mixed), and normalized, modified, polarized radiance (L_{nmp}) at 865 nm. L_{nmp} is defined as follows (C.-Labonnote et al. 2001):

$$L_{nmp} = \frac{\pi L_p}{E_s} \frac{\cos\theta_s + \cos\theta_v}{\cos\theta_s}, \quad (1)$$

where subscript *s* represents the solar zenith and azimuth angles and subscript *v* is the viewing angle. E_s is the TOA solar irradiance. Since L_{nmp} is normalized by the incident irradiance, it is a dimensionless quantity, and will be called polarized reflectance in this paper. L_p is the linearly polarized radiance, defined as:

$$L_p = \pm\sqrt{Q^2 + U^2}, \quad (2)$$

where the sign is determined by the angle between the polarization vector and the normal to the scattering plane (C.-Labonnote et al. 2001).

One full day of global PARASOL observations from 1 August 2007 are used in this study, representing 14 orbits. The product is filtered to retain PARASOL pixels over the ocean with 100% cloud cover within the 18x18 km spatial area. Additionally, the cloud phase indicated in the Level-2 product must be ice, and there must be at least 7 different viewing geometries observed by PARASOL for a given pixel to be included in this study. The total number of pixels before filtering was 933,129, with 69,481 pixels (just over 7%) remaining after filtering using the criteria described above.

2.2 Adding-Doubling Radiative Transfer model

The vector adding-doubling RT model developed by de Haan et al. (1987) is used to provide the intensity and polarization state of radiation at the top of the atmosphere (TOA) containing a layer of modeled ice cloud with given scattering properties. A mid-latitude summer atmospheric profile based on the U.S. standard atmosphere is used in the calculations, assuming a total Rayleigh optical depth of 0.01587 at 865 nm (Tomasi et al. 2005). A single-layer ice cloud with optical depth 5 is assumed at a level of 9 km for all simulations, and they are done over a refractive ocean surface with an index of refraction value of 1.33. The viewing geometries of 3000 randomly selected PARASOL pixels from 1 August 2007 are used as the input geometries to produce the simulated polarized reflectance. The Stokes vector output at TOA is used to produce the simulated polarized reflectance L_{nmp}, the same quantity from PARASOL observations.

2.3 Spherical Albedo Differences (SAD) test

To test the angular coherence of cloud spherical albedo, a SAD analysis (C.-Labonnote et al. 2001) is performed. The cloud optical thickness is derived from the different observation angles available from PARASOL and then the microphysical and optical properties in a chosen cloud model are used to infer the spherical albedo (for details on the PARASOL retrieval method, see Buriez et al. (1997)). If the cloud model described the optical properties perfectly, the spherical albedo would be independent of scattering angle. Any differences observed between the multiangle retrievals of cloud spherical albedo provide information about the angular consistency of the assumed cloud model. It is important to note that the cloud model actually includes two separate assumptions, one on cloud macrophysical properties (cloud is plane-parallel homogeneous) and the other on microphysical properties

(particle size and habit distribution). Both could potentially impact the angular distribution of reflectance, but it is assumed that the cloud microphysics (through the ice phase function) is the dominant factor governing rapid changes in the cloud bidirectional reflectance distribution function (BRDF) and bidirectional polarization distribution function (BPDF), especially when an analysis is performed over a wide range of view and sun zenith angles, and subsequently scattering angles.

2.4 Ice Bulk Scattering Properties

To calculate the reflected polarized light using the adding-doubling model, the bulk scattering properties of the ice particles within the simulated cloud are required. For this study, the single-scattering properties of 9 different ice habits (shapes) are obtained at a wavelength of 865 nm with a combination of the discrete dipole approximation method (DDA) and the improved geometric optics method (IGOM) (Yang et al. 2012). The 9 habits are droxtals, solid and hollow columns, solid and hollow 3D bullet rosettes, plates, aggregate of columns, and a small and large aggregate of plates, whose geometries are illustrated in Fig. 1. The single-scattering properties are derived assuming random orientation of the particles. The ice particles may have smooth, moderately roughened, and severely roughened surfaces. The method for calculating the surface roughness is to randomly lift and tilt the facet of the ice particle. The parameter σ describes the level of roughness, with $\sigma = 0$ being smooth, 0.05 representing moderately roughened particles, and a level of $\sigma = 0.5$ for severely roughened ice particles (Yang; Liou 1998).

The procedure for calculating the bulk scattering properties follows that of Baum et al. (2005b). For an ice cloud composed of a mixture of habits, the bulk scattering properties are obtained from integration over the habit distribution, the size distribution, the spectral

response function of the PARASOL imager, and the solar spectrum. The size distributions used in the calculations come from a variety of field campaigns including CRYSTAL-FACE, TRMM, ARM, SCOUT, and others (Baum et al. 2011).

The average single-scattering phase matrix is computed in the following way:

$$P(\Theta) = \frac{\int_{\lambda_1}^{\lambda_2}\int_{D_{min}}^{D_{max}}\left[\sum_{h=1}^{M} P_h(\Theta,D,\lambda)\sigma_{sca,h}(D,\lambda)f_h(D)\right]n(D)F_s(\lambda)S(\lambda)\,dD\,d\lambda}{\int_{\lambda_1}^{\lambda_2}\int_{D_{min}}^{D_{max}}\left[\sum_{h=1}^{M}\sigma_{sca,h}(D,\lambda)f_h(D)\right]n(D)F_s(\lambda)S(\lambda)\,dD\,d\lambda}, \qquad (3)$$

where M is the number of habits, D is the particle diameter, $n(D)$ is the number density, $F_s(\lambda)$ is the spectral response function, and $S(\lambda)$ is the solar flux. The scattering cross section is σ, and the habit fraction is defined so that

$$\sum_{h=1}^{M} f_h(D) = 1. \qquad (4)$$

The effective diameter D_{eff} is proportional to the ratio of the total volume to the total projected area and is given by the following expression:

$$D_{eff} = \frac{3}{2}\frac{\sum_{h=1}^{M}\left[\int_{D_{min}}^{D_{max}} V_h(D)f_h(D)n(D)\,dD\right]}{\sum_{h=1}^{M}\left[\int_{D_{min}}^{D_{max}} A_h(D)f_h(D)n(D)\,dD\right]}. \qquad (5)$$

The bulk asymmetry parameter g and bulk scattering cross sections are calculated in the same manner as the phase matrix above.

The resulting phase functions tend to be strongly peaked in the forward direction, making it necessary to truncate this peak before performing the radiative transfer calculations. The δ-fit method (Hu et al. 2000) is used to truncate the forward peak, and the other phase matrix

elements are then normalized by the truncated phase function. The truncated, normalized bulk scattering phase matrix is then used in the RT calculations. In addition, the optical thickness, scattering cross section, and asymmetry parameter are all adjusted after the truncation based on the similarity principle (Joseph et al. 1976).

For this study, the habit distribution used in MODIS collection 5 retrievals is considered (henceforth referred to as C5M), along with a general habit mixture (GHM) proposed for future MODIS retrievals. The single-scattering properties for the single habits used in the GHM are also used in simulations and the results analyzed. The MODIS C5M includes the following six habits: solid columns, hollow columns, solid 3D bullet rosettes, droxtals, plates, and an aggregate of solid columns. Droxtals are used for the smallest sizes, while columns, plates, and bullet rosettes make up the middle sizes. Aggregates of solid columns and solid bullet rosettes are used for the largest ice particle sizes in the size distribution considered. All of the ice habits considered are smooth-surfaced in C5M, with the exception of the aggregate of solid columns, which is severely roughened.

In addition to the six habits in MODIS C5, the proposed GHM includes 3D hollow bullet rosettes, and a small and large aggregate of plates. In contrast to the C5M, the habits transition linearly with particle size; this prevents potential artifacts in the bulk scattering properties that could arise from switching habits abruptly. Fig. 2 shows the GHM distribution of habits as a function of particle diameter.

The hope is that a given habit distribution will provide results for inferred ice cloud optical thickness and particle size that are consistent between sensors taking measurements at different wavelengths. One way of assessing the consistency in the expected retrievals is to examine results using the polarized reflectance and total radiance measurements from

PARASOL. In this study, the polarized and total radiances are simulated using the bulk scattering properties as input to a RT model, whereupon the simulated radiances are compared to those from PARASOL.

3. Results

In this section we present the results of simulations of polarized reflectance based on bulk scattering models derived using the C5M, the GHM, and selected individual habits. The simulations of polarized reflectance are compared to polarized reflectance measured by PARASOL on 1 August 2007. Fig. 3(a) shows simulated polarized reflectance using the C5M assuming D_{eff} = 60 μm and τ = 5 (black dots) superimposed over the measured polarized reflectances from PARASOL (color contours). The color contours represent the smoothed frequency of PARASOL measurements, with blue (red) displaying lower (higher) frequencies of observed reflectances. The black dots are based on a set of 3000 points defined by the viewing geometry from individual PARASOL pixels. Because the same scattering angle may be obtained from different combinations of viewing zenith, solar zenith, and relative azimuth angles, a given scattering angle may have several simulated polarized reflectance points; this leads to the dispersion in the simulation results seen in Fig. 3 and following figures. The simulated reflectances clearly do not match well with the measurements over the range of scattering angles.

Fig. 3b shows the simulation results that are obtained if the GHM is adopted assuming smooth particles, for the same conditions of D_{eff} = 60 μm and τ = 5. To be clear, the results assume smooth-faceted particles similar to the C5M but employ the additional three habits, and are based on linearly-changing habit fractions. The results indicate that increasing the

number of ice habits in the mixture and changing their fractions does not improve the comparison with the measured polarized reflectance data.

Another parameter to consider is surface roughness. Fig. 3(c) shows the results for the GHM with a moderate level of surface roughness, once again with D_{eff} = 60 μm and τ = 5. Note that the peaks are smoothed out and the fit to observed polarized reflectance improves over that for smooth particles, but the values are still too high, especially for scattering angles from 60 – 130 degrees.

Fig. 3d shows the results for the GHM with severely roughened particles, once again with D_{eff} = 60 μm and τ = 5. When severe surface roughness is used in simulations, the simulated and measured polarized reflectances are much closer over the range of scattering angles. The severely roughened particles provide the closest fit to the observed polarized reflectances and indicates that the bulk ice cloud optical properties should incorporate at least a certain degree of surface roughness in their derivation.

The dramatic change in polarized reflectances observed in the simulations from particle roughening comes from the removal of peaks in the scattering phase matrix as seen in Fig. 4. The phase function becomes nearly featureless when assuming severe surface roughness. The degree of linear polarization P_{12} becomes almost featureless as well, with a downward slope over the range of scattering angles observed from polar-orbiting sensors. This smoothing of the scattering phase matrix by the roughening of the ice surface is discussed in more detail in Baum et al. (2010).

Fig. 3 showed that in comparison with the PARASOL polarization data from Aug. 1st 2007, the MODIS C5M model (smooth particles) for D_{eff} = 60 μm provided a poor fit to the observations, while the model at D_{eff} = 60 μm based on the GHM assuming severely

roughened ice particles most improved the comparison with measurements. To determine whether the ice cloud optical models based on the GHM provide a match to observations over a range of D_{eff} that might be encountered in ice cloud retrievals, simulations were performed for optically thick ice clouds (τ = 5) at D_{eff} = 30, 50, 70, and 90 μm, all with severely roughened particles. Fig. 5 shows the results for all four cases. Though there is a slight variation with D_{eff}, the simulated polarized reflectances compare favorably with the PARASOL measurements.

The question we now address is whether an individual habit can be used instead of a habit mixture. Fig. 6 shows the simulated polarized reflectance again assuming D_{eff} = 60 μm and τ = 5 for each of the nine habits shown in Fig. 1. Interestingly, the hollow particles tend to most closely match with observations, and the hollow bullet rosettes in particular do well. Plates have simulated polarized reflectance that is too large at small scattering angles from 60° – 120°, while solid columns and droxtals have polarized reflectance values that are too small over roughly the same range. Even though some single habits can provide a good fit to the observed PARASOL measurements when severe surface roughness is assumed, it was shown in Baum et al. (2011) that the GHM model compares well with the microphysical properties provided by in situ data, specifically with regards to ice water content (IWC) and median mass diameter.

The results of the SAD analysis for the general habit mix as well as several single habits are shown in Fig. 7 for D_{eff} = 60 μm. The desired result for a given model is that it should minimize the normalized relative spherical albedo differences. Additionally, the residual quantities should not have any strong angular dependence. When a least square linear fit is performed through the residual, the correlation coefficient should be high and the slope

should be as small as possible, indicating no angular dependence. The top three panels in Fig. 7 illustrate the impact of surface roughening with the GHM models, indicating that it does reduce angular biases in cloud optical depth retrievals. The bottom three panels in combination with the top right for the severely roughened particle model illustrate the impact of particle habit distributions. It can clearly be seen that details of the habit distribution are somehow of second order when surface roughening is introduced but some strong differences remain visible, especially at side scattering angles (below 90 degrees).

The top panel of Fig. 8 shows the RMS of relative spherical albedo differences over the full range of effective diameters for the models under consideration. All the models evaluated tend to provide comparable relative SAD RMS over the two different days of data tested, with the results for Aug. 1st, 2007 shown here. The GHM tends to be slightly better at larger effective diameters in terms of RMS. The hollow bullet rosette and solid column (both severely roughened) have an almost constant SAD RMS regardless of effective diameter, and provide the smallest RMS for $D_{eff} \leq 30$ μm.

The middle and lower panels of Fig. 8 show the slope of the linear regression performed through the SAD residual as well as the linear correlation coefficient. The various models present significantly different behaviors in terms of the slope as a function of effective diameter. The solid column (severely rough) has the least variation while the slope from the GHM actually changes sign when going from small to large D_{eff}. The linear correlation coefficients indicate, however, that the solid column still exhibits a significant angular variability that is not present in the PARASOL observations. Similarly, the solid bullet rosette (severely roughened) has small slope values but the corresponding linear correlation

coefficients are low, indicating that angular biases created by the model assumption are highly variable (i.e., not linearly correlated with scattering angle).

4. Summary

This study investigates the fit of simulated polarized reflectance at 0.865 μm to PARASOL multi-angle polarized reflectance observations using different ice habit mixtures and values of ice particle surface roughness. A spherical albedo difference (SAD) test is used to test the angular consistency of the ice models. The MODIS collection 5 ice habit mixture (C5M), a new general habit mixture (GHM), and individual habits are used to simulate polarized reflectances. The surface roughness can be smooth, moderately rough, or severely rough.

The MODIS C5M models result in a poor fit of the simulated polarized reflectances to the observed polarized reflectances, and add to the evidence that the assumption of smooth particles may be inadequate for global retrieval of ice properties. With the GHM, which uses three additional habits and has the habit fractions changing linearly with particle size, the assumption of smooth-faceted ice crystals also provide a poor comparison with PARASOL. As the roughening increases, however, the comparison of simulated to measured polarized reflectances improves across a range of effective diameters and scattering angles.

With bulk scattering models based on the GHM and severely roughened particles, the simulated to measured polarized reflectances remain comparable for a range of effective diameter values from 30 to 90 μm. This range of D_{eff} values is encompassed from current MODIS retrievals (although these are based on smooth particles).

There are individual ice habits that can match the observed PARASOL polarized reflectance data, including hollow columns and hollow bullet rosettes. However, an ensemble

mix of ice habits better matches IWC and median mass diameter in situ data (Baum et al. 2005a). As cloud retrieval teams decide what bulk scattering models to adopt in future operational and research efforts, these results will hopefully provide useful guidance.

From the SAD analysis, it is difficult to decide which model is the best in all respects. It is clear that surface roughness does improve significantly the different metrics used to quantify the adequacy of a model in terms of minimizing systematic angular biases occurring when deriving cloud optical thickness. It should be noted that moderate roughening tends to provide smaller values of slope (i.e., less angular dependency) than severe roughening. Moderate roughening also gives slightly better relative SAD RMS values but at the same time does not yield as high a linear correlation as does severe roughening. With regards to the details of the habits used to build the size distribution, it seems that the GHM has some advantages, it also has some variations with effective diameter. Hollow bullet rosettes and solid bullet rosettes tend to provide slightly worse results but are more homogeneous over the range of effective diameters.

With regard to the varying results over effective diameter, it must be noted that a single unique model (habit + size) has been used to process the measured PARASOL data each time. No attempt has been made to select the best effective size for a given habit distribution, and in fact it would not be very surprising that the best microphysical model could indeed depend strongly on particle size.

Previous work by Knap et al. (2005) found that the imperfect hexagonal monocrystal (IMP) and inhomogeneous hexagonal monocrystal (IHM) models simulated adequately the polarized reflectance observed globally on 10 November 1996. The advantage of the GHM model considered in the current study is that it compares well with IWC and median mass

diameter inferred from in situ microphysical data, and it also adequately simulates global polarized reflectance observed on 1 August 2007.

From all the habit-based models considered in this study, the one which provides the best match to the polarized reflectance observations and gives reasonable results in the SAD analysis is the general habit mixture with severe particle roughening. It is suggested that this model would potentially be an adequate choice for future global ice cloud retrievals using MODIS, and a significant improvement over the C5M models adopted for Collection 5 operational processing.

Acknowledgements

We thank the ICARE Data and Services Center for providing access to the data used in this study, and for tools used in the data processing. This study was supported by NASA grants NNX10AL55G and NNX11AK37G. Bryan Baum and Ping Yang also acknowledge the support of NASA grant NN11AF40G.

References

Baran, A. J., 2009: A review of the light scattering properties of cirrus. *JQSRT*, **110,** 1239-1260.

Baum, B. A., A. J. Heymsfield, P. Yang, and S. T. Bedka, 2005a: Bulk scattering properties for the remote sensing of ice clouds. part I: microphysical data and models. *J. Appl. Met. Clim.*, **44,** 1885-1895

Baum, B. A., P. Yang, Y. X. Hu, and Q. Feng, 2010: The impact of ice particle roughness on the scattering phase matrix. *JQSRT*, **111,** 2534-2549.

Baum, B. A., P. Yang, A. J. Heymsfield, S. E. Platnick, M. D. King, Y. X. Hu, and S. T. Bedka, 2005b: Bulk scattering properties for the remote sensing of ice clouds. part II: narrowband models. *J. Appl. Met. Clim.*, **44,** 1896-1911

Baum, B. A., and Coauthors, 2011: Improvements in shortwave bulk scattering and absorption models for the remote sensing of ice clouds. *J. Appl. Met. Clim.* , **50,** 1037-1056

Buriez, J. C., and Coauthors, 1997: Cloud detection and derivation of cloud properties from POLDER. *Int. J. Rem. Sens.*, **18,** 2785-2813.

C.-Labonnote, L., G. Brogniez, J. C. Buriez, and M. Doutriaux-Boucher, 2001: Polarized light scattering by inhomogeneous hexagonal monocrystals: Validation with ADEOS-POLDER measurements. *J. Geophys. Res.* , **106,** 12,139-153

Chepfer, H., G. Brogniez, and Y. Fouquart, 1998: Cirrus clouds' microphysical properties deduced from POLDER observations. *JQSRT*, **60,** 375-390.

de Haan, J. F., P. B. Bosma, and J. W. Hovenier, 1987: The adding method for multiple scattering calculations of polarized light. *Astron. Astrophys.*, **183,** 371-391.

Deschamps, P., F. M. Breon, M. Leroy, A. Podaire, A. Bricaud, J. C. Buriez, and G. Seze, 1994: The POLDER mission: instrument characteristics and scientific objectives. *IEEE Trans. Geosci. Rem. Sensing* **32,** 598-615.

Fougnie, B., G. Bracco, B. Lafrance, C. Ruffel, O. Hagolle, and C. Tinel, 2007: PARASOL in-flight calibration and performance. *Appl. Optics* **46,** 5435-5451

Hu, Y. X., B. Wielicki, B. Lin, G. Gibson, S. C. Tsay, K. Stamnes, and T. Wong, 2000: d-fit: a fast and accurate treatment of particle scattering phase functions with weighted singular-value decomposition least-squares fitting. *JQSRT*, **65,** 681-690.

Joseph, J. H., W. J. Wiscombe, and J. A. Weinman, 1976: Delta-Eddington approximation for radiative flux-transfer. *J. Atmos. Sci.*, **33,** 2452-2459.

Knap, W. H., L. C.-Labonnote, G. Brogniez, and P. Stammes, 2005: Modeling total and polarized reflectances of ice clouds: evaluation by means of POLDER and ATSR-2 measurements. *Appl. Optics*, **44,** 4060-4073.

Liou, K. N., 1986: Influence of cirrus clouds on weather and climate processes: a global perspective. *Mon. Wea. Rev.*, **114,** 1167-1198.

Nazaryan, H., M. P. McCormick, and W. P. Menzel, 2008: Global characterization of cirrus clouds using CALIPSO data. *J. Geophys. Res.*, **113,** D16211.

Tomasi, C., V. Vitale, B. Petkov, A. Lupi, and A. Cacciari, 2005: Improved algorithm for calculations of Rayleigh-scattering optical depth in standard atmospheres. *Appl. Optics* **44,** 3320-3341

Yang, P., and K. N. Liou, 1998: Single-scattering properties of complex ice crystals in terrestrial atmosphere. *Contr. Atmos. Phys.* , **71,** 223-248.

Yang, P., L. Bi, B. A. Baum, K. N. Liou, G. W. Kattawar, and M. Mishchenko, 2012: Spectrally consistent scattering, absorption, and polarization properties of atmospheric ice crystals at wavelengths from 0.2 μm to 100 μm. *J. Atmos. Sci.*, **Submitted**.

List of Figures

Fig 6: Simulated polarized reflectance calculated using nine different single ice habits, all at an effective diameter of 60 μm: a) droxtal; b) solid 3D bullet rosette; c) hollow 3D bullet rosette; d) hollow column; e) solid column; f) plate; g) aggregate of columns; h) small aggregate of plates; i) large aggregate of plates. An optically thick ($\tau = 5$) ice cloud is used in the simulation and the ice particles are severely rough. Color contours are density of PARASOL polarized reflectance data from 1 August 2007, and black dots are simulations.

Fig. 7: Results of the relative SAD analysis for the general habit mix (GHM) and selected single habits: a) GHM smooth; b) GHM moderately rough; c) GHM severely rough; d) solid column, severely rough; e) solid 3D bullet rosette, severely rough; f) hollow 3D bullet rosette, severely rough. Color contours are density of observations normalized to the maximum value, and blue dots are the number of samples at that scattering angle (scale on the right). One day of global observations from 1 August 2007 is used.

Fig. 8: Panel (a) shows the RMS of relative spherical albedo differences (SAD) for the various models; panel (b) shows the slope of linear regression for relative spherical albedo differences; and panel (c) shows the correlation coefficients of linear regression for relative spherical albedo differences. One day of global observations from 1 August 2007 is used.

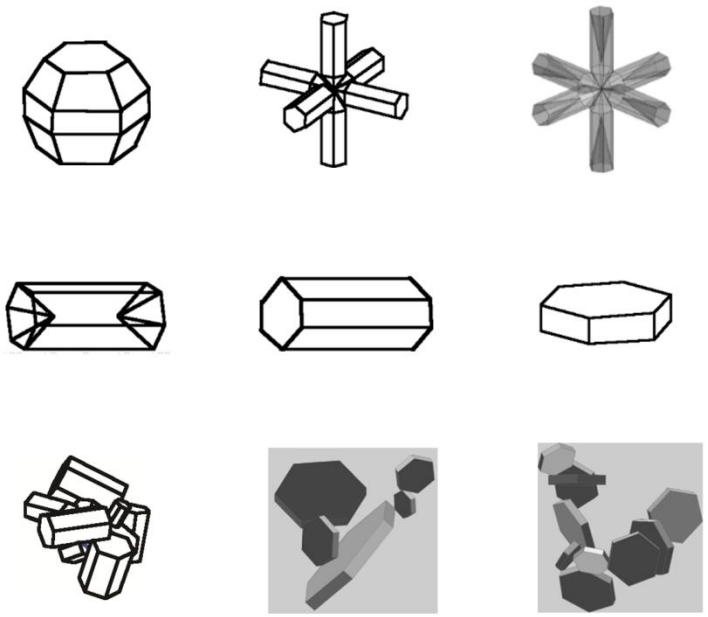

Fig. 1.

The 9 ice habits used in the general habit mix. The top row shows a droxtal plus solid and hollow 3D bullet rosettes, the middle row shows a hollow and a solid column and a plate, and the bottom row shows an aggregate of columns, a 5-member aggregate of plates, and a 10-member aggregate of plates.

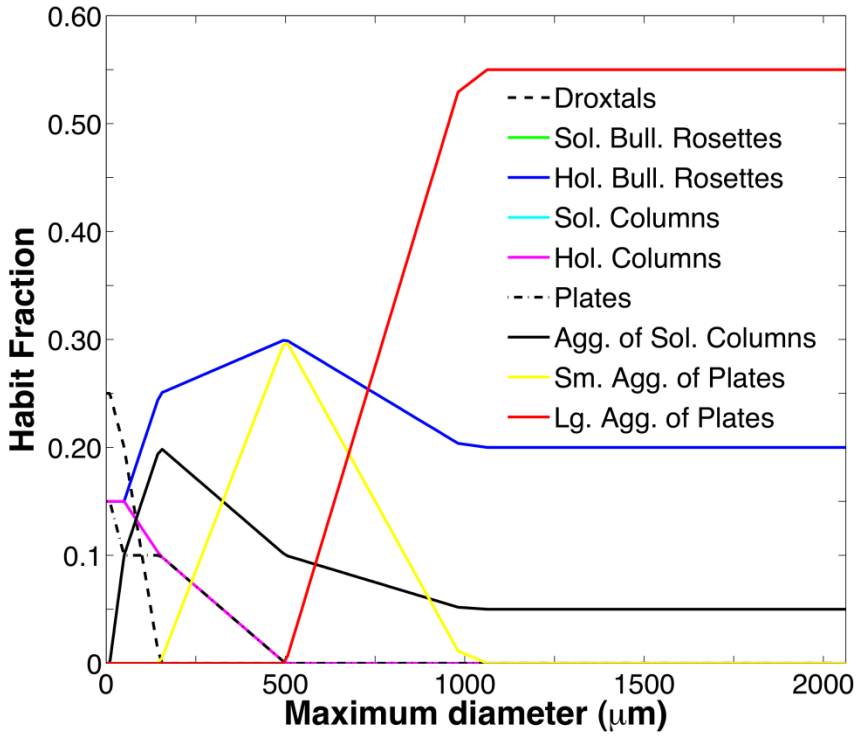

Fig. 2.

Ice crystal habit fraction as function of diameter for the general habit mix used in this study. The habit fractions remain the same past the maximum size shown in this plot. These fractions are used when calculating bulk scattering properties using measured particle size distributions.

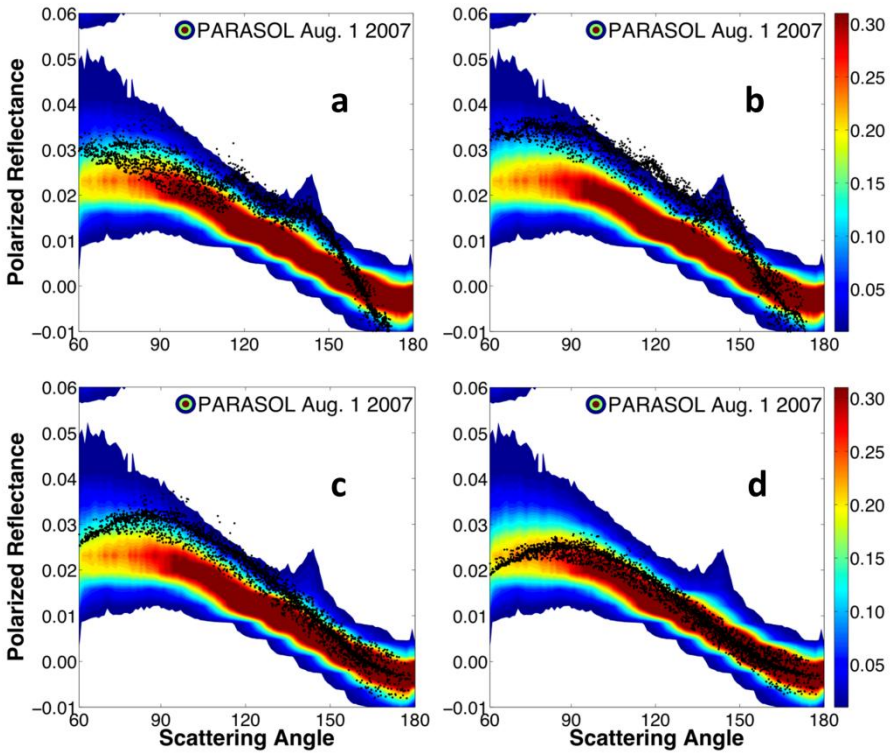

Fig. 3.

Simulated polarized reflectance calculated at an effective diameter of 60 μm with an optically thick (τ = 5) ice cloud for a) MODIS collection 5 model; b) general habit mix with smooth ice particles; c) general habit mix with moderately rough ice particles; d) general habit mix with severely rough ice particles. Color contours are density of PARASOL polarized reflectance data from 1 August 2007, and black dots are simulations.

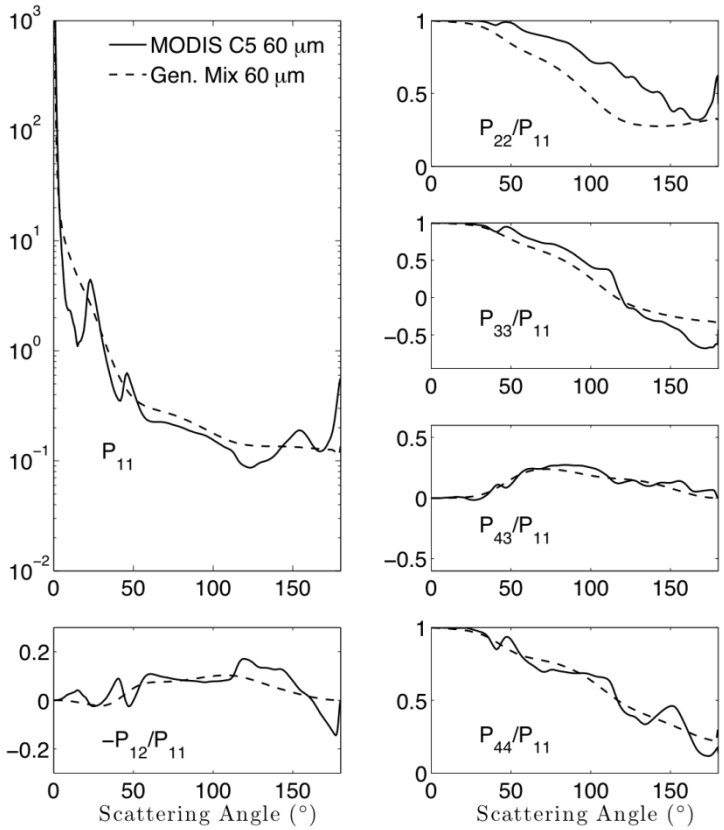

Fig. 4.

Comparison of the phase matrix components of the MODIS collection 5 ice habit mix and the new general habit mix with severe surface roughness at an effective diameter of 60 μm.

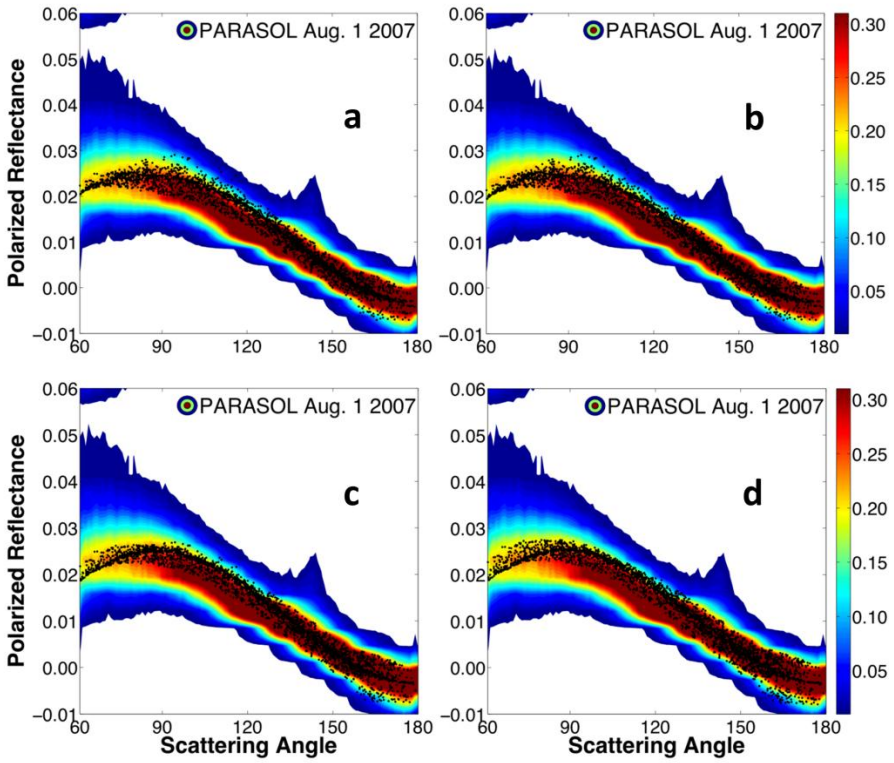

Fig. 5.

Simulated polarized reflectance calculated using the new general habit mix at four different effective diameters: a) 30 μm; b) 50 μm; c) 70 μm and d) 90 μm. An optically thick ($\tau = 5$) ice cloud is used in the simulation and the ice particles are severely rough. Color contours are density of PARASOL polarized reflectance data from 1 August 2007, and black dots are simulations.

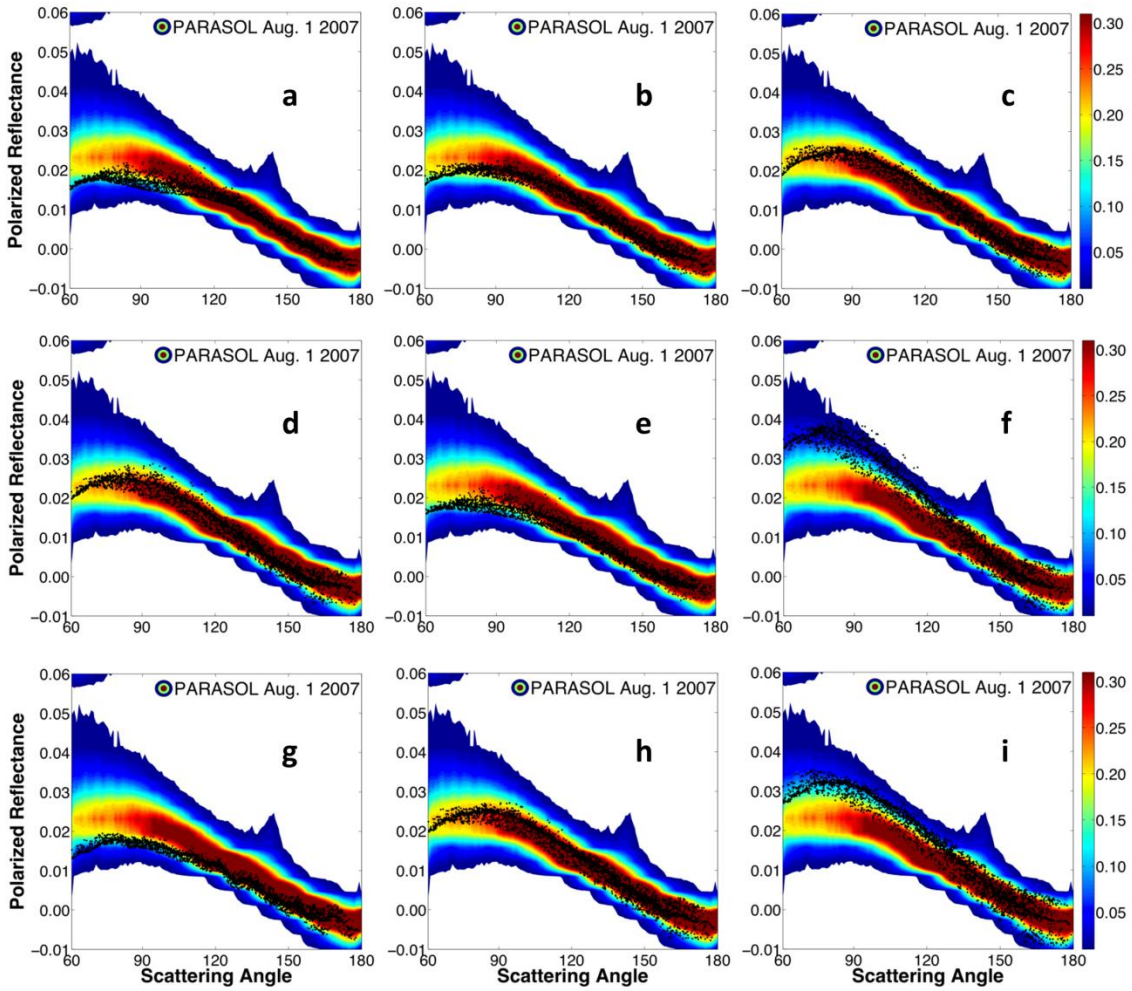

Fig 6.

Simulated polarized reflectance calculated using nine different single ice habits, all at an effective diameter of 60 μm: a) droxtal; b) solid 3D bullet rosette; c) hollow 3D bullet rosette; d) hollow column; e) solid column; f) plate; g) aggregate of columns; h) small aggregate of plates; i) large aggregate of plates. An optically thick ($\tau = 5$) ice cloud is used in the simulation and the ice particles are severely rough. Color contours are density of PARASOL polarized reflectance data from 1 August 2007, and black dots are simulations.

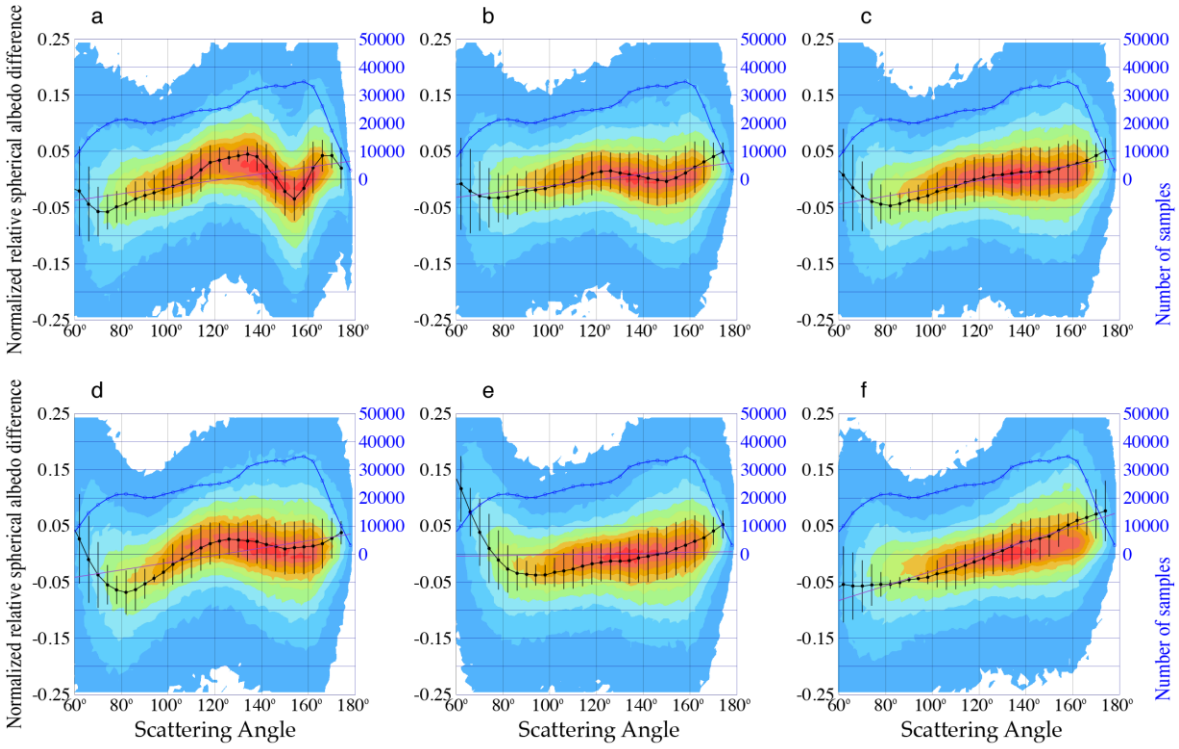

Fig. 7

Results of the relative SAD analysis for the general habit mix (GHM) and selected single habits: a) GHM smooth; b) GHM moderately rough; c) GHM severely rough; d) solid column, severely rough; e) solid 3D bullet rosette, severely rough; f) hollow 3D bullet rosette, severely rough. Color contours are density of observations normalized to the maximum value, and blue dots are the number of samples at that scattering angle (scale on the right). One day of global observations from 1 August 2007 is used.

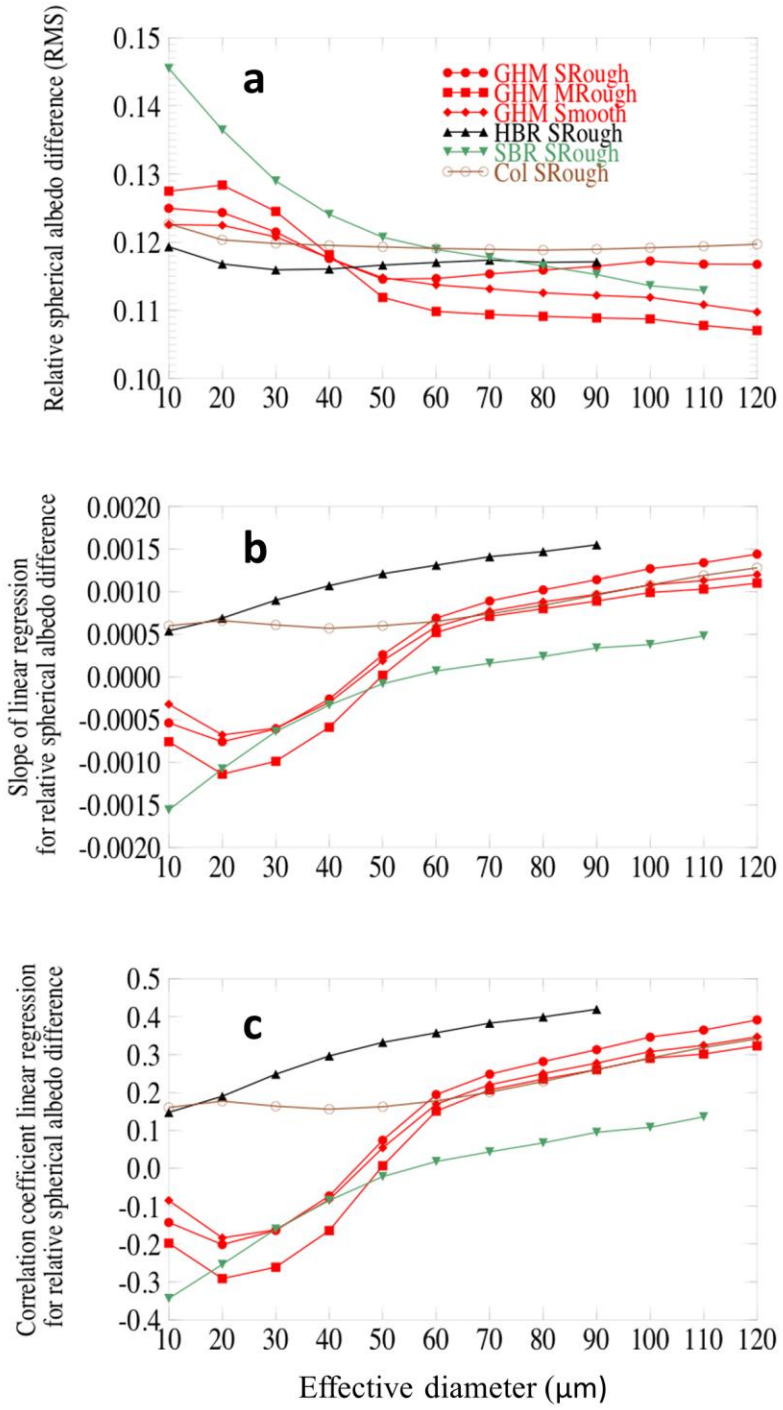

Fig. 8

Panel (a) shows the RMS of relative spherical albedo differences (SAD) for the various models; panel (b) shows the slope of linear regression for relative spherical albedo differences; and panel (c) shows the correlation coefficients of linear regression for relative spherical albedo differences. One day of global observations from 1 August 2007 is used.